NANOMATERIALS AND NANOTECHNOLOGY

Nanomaterials and Nanotechnology
Volume 9: 1–8

DOI: 10.1177/1847980419832724
journals.sagepub.com/home/nax
SAGE

Evaluation of fiber-optic phase-gradient meta-tips for sensing applications

M Principe[1,2], M Consales[3], G Castaldi[3], V Galdi[3], and A Cusano[3]

Abstract

Recently, within the emerging framework of "lab-on-fiber" technologies, we successfully demonstrated the integration of phase-gradient plasmonic metasurfaces on the tip of an optical fiber. The resulting optical-fiber "meta-tips" promise to empower the typical fiber-optics application scenarios (e.g. sensing, telecommunications, imaging, etc.) with the advanced light-manipulation capabilities endowed by metasurfaces. Here, we explore more in detail the possibility to exploit this platform in label-free biological or chemical sensing applications. Specifically, we carry out a parametric study of the surface sensitivity and show that phase-gradient metasurfaces generally outperform their gradient-free counterparts, without imposing additional fabrication complexity. Therefore, the phase gradient can be effectively exploited as an additional degree of freedom in the design of high-sensitivity devices.

Keywords

Metasurfaces, lab-on-fiber technology, sensing, surface waves, plasmonic nanosensors

Date received: 14 June 2018; accepted: 29 January 2019

Topic: Nanooptics and Nanophotonics
Topic Editor: Dr Paola Prete
Associate Editor: Professor Mateusz Smietana

Introduction

Plasmonic nanosensors, exploiting the local electromagnetic field enhancement and the ultra-sensitivity of surface plasmon resonances to variations of the surrounding environment, nowadays represent the state-of-the-art platforms for biological and chemical sensing applications. Nevertheless, the field is rapidly evolving driven by the strong push for improved sensitivity, in terms of increased wavelength shift and/or spectral selectivity of the resonances.[1,2] Typical routes to enhance the sensitivity mainly rely on the optimized design of the nanostructure, as well as tailoring the plasmon coupling and inducing amplification effects via nanoparticle growth.[3]

Moreover, recently emerged technological paradigms such as "lab-on-fiber"[4–6] strongly push toward the integration of nanoplasmonic sensing platforms in optical fibers, leading to a novel generation of advanced "all-in-fiber" miniaturized optrodes.

Within this framework, in our previous study,[7] we demonstrated the first integration of phase-gradient plasmonic metasurfaces (MSs) on the tip of an optical fiber. The resulting fiber-optic "meta-tips" represent a major breakthrough in the lab-on-fiber technology roadmap. Optical MSs are 2-D implementations of metamaterials,[8] much easier to fabricate than their 3-D counterparts, and allow to integrate exceptional light-manipulation capabilities within miniaturized photonics platforms. Our proposed meta-tips provide a very promising bridge between the fiber-optic technologies and the emerging

[1] Physics Department, University of Salerno, Fisciano (SA), Italy
[2] Centro Studi e Ricerche Enrico Fermi, Roma, Italy
[3] Department of Engineering, University of Sannio, Benevento, Italy

Corresponding author:
Maria Principe, Physics Department, University of Salerno, Via Giovanni Paolo II 132, I-84084 Fisciano (SA), Italy.
Email: principe@unisannio.it

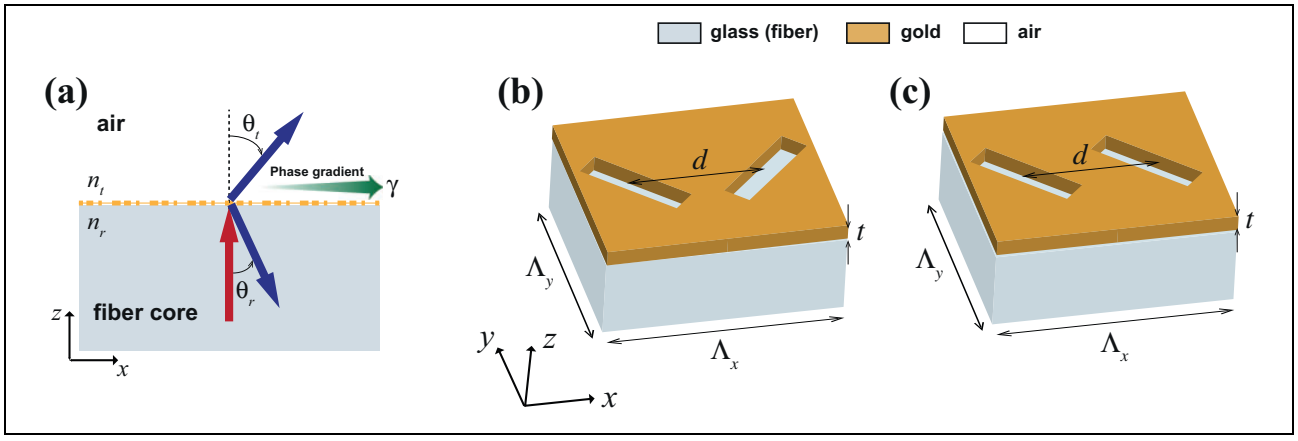

Figure 1. (a) Schematic of a fiber-optic meta-tip. (b), (c) Geometry of the phase-gradient MS macrocell and the corresponding (gradient-free) benchmark, respectively; both of them are based on aperture antennas on a gold layer. MS: metasurface.

field of "flat" optics and photonics,[9–11] with a plethora of potential applications to imaging,[12,13] sensing,[14,15] processing, and computing.[16,17]

Inspired by reflect/transmit-array radio-frequency antennas,[18,19] optical MSs are based on 2-D arrays of heterogeneous resonators which can locally impart abrupt phase and amplitude variations in an impinging wave front. Reliance on plasmonic[20] or high-index dielectric nanoantennas[21] allows maintaining a deeply subwavelength profile. After the groundbreaking proposal by Yu et al.,[22] where generalized Snell's laws were formulated and implemented via MSs based on V-shaped plasmonic nanoantennas, the field of MSs has rapidly developed and currently represents one of the most active and fast-pacing research areas (see, e.g. previous studies[23–35] for a sparse sampling of key contributions and recent reviews).

As the interest in metamaterials and MSs for sensing applications is steadily growing,[14,36] our work[7] put forward the idea of exploiting phase-gradient MSs, showing that the phase modulation represents an important additional degree of freedom, which can yield sensible enhancements of the surface sensitivity with little or no additional complexity.

Starting from this promising result, this article is entirely devoted to the study of the effect of the phase gradient on the local sensitivity and to the comparison of the sensitivity of phase-gradient MSs with the corresponding gradient-free benchmark. This study will aid in the design of a high-sensitivity meta-tip for label-free biological and chemical sensing applications.

MS design

Our fiber-optic meta-tip[7] is schematized in Figure 1(a). We assume a phase-gradient MS located at the interface (in the transverse x-y plane) separating the incidence region (fiber) and an exterior medium. The transmission (θ_t) and reflection (θ_r) angles are ruled by the generalized Snell's laws.[22] For normal incidence (along the z-direction), we obtain

$$\sin\theta_t = \frac{1}{n_t}\frac{\lambda_0}{2\pi}\gamma, \quad \sin\theta_r = \frac{1}{n_r}\frac{\lambda_0}{2\pi}\gamma \tag{1}$$

where $n_{t/r}$ is the refractive index of the transmission/incidence region, λ_0 is the operation wavelength, and γ is the phase gradient along the x-direction (the phase gradient along y is assumed to be zero). By properly tuning the phase gradient, it is possible to attain arbitrary values of $\theta_{t/r}$ for normal incidence.

The generalized Snell's laws have also been exploited to convert a propagating plane wave into a surface wave.[37,38] However, it was recently demonstrated[39,40] that this approach, based on a simple phase correction stemming from ray optics, suffers from very low efficiency due to the local impedance mismatch on the surface. Hence, one should consider the full-wave electromagnetic problem and solve for the surface impedance required for perfect conversion.[39–41] In previous research,[40,41] it was shown that, to realize perfect refraction with lossless constituents, spatial dispersion is needed in the form of artificial magnetism and bianisotropic omega coupling.[42]

Our chosen configuration, based on a single layer of plasmonic antennas, does not provide enough degrees of freedom to tailor the needed polarizabilities. Therefore, acknowledging the implied limitations, we followed the simplified approach based on the generalized Snell's laws.

Accordingly, to drive a normally impinging plane wave to the evanescent range (surface wave) in transmission, we need to exceed the grazing condition $\theta_t = 90^\circ$. From equation (1), this can be realized with a sufficiently large phase gradient, namely

$$\gamma \geq n_t \frac{2\pi}{\lambda_0} \tag{2}$$

A similar condition applies for the reflection scenario. In our MS, the phase gradient is implemented by an infinite

repetition along x and y of a $1 \times N$ macrocell, where the full phase range of 2π along x is sampled by N nanoantennas, featuring a uniform phase difference $\Delta\phi$ in the transmission (and reflection) coefficients, separated by a distance d, so that $\gamma = \frac{\Delta\phi}{d} = 2\pi/\Lambda_x$, where $\Lambda_x = N \cdot d$ is the period of the MS array along x. We fix the period along y to $\Lambda_y = 1$ μm. In this case, the surface-wave condition in equation (2) can be equivalently written as

$$\Lambda_x = Nd = \frac{2\pi d}{\Delta\phi} \leq \frac{\lambda_0}{n_t} \tag{3}$$

The nanoantenna distance d cannot be arbitrarily reduced beyond a certain value to limit the intercoupling effects. For our wavelength range of interest (1.2 to 2.4/μm), we estimated from numerical simulations that a minimum distance of 100nm must be kept from any antennas. Hence, to further increase the phase gradient, we can reduce the number N of antennas per macrocell, which is equivalent, at fixed d, to increasing the sampling step of the phase profile, $\Delta\phi$. At fixed γ, equations (2) and (3) can be solved for the minimum wavelength at which the transmitted field couples to a surface wave, namely

$$\lambda_{SW} = n_t \frac{2\pi}{\gamma} = n_t \Lambda_x \tag{4}$$

In a similar way, the minimum wavelength at which the reflected field couples to a surface wave can be evaluated.

We highlight that λ_{SW} in equation (4) coincides with the first Rayleigh anomaly, due to the periodic nature of the grating.[43] Recalling the phase-matching condition for the optimal launch of a surface plasmon polariton (SPP)[44]

$$\pm k_{SPP} = \frac{\Delta\phi}{d} + \nu\frac{2\pi}{d} \tag{5}$$

where ν is the SPP launching order; it also appears that λ_{SW} in equation (4) satisfies this condition for $\nu = 0$.

As in the earlier study,[7] we considered Babinet-inverted plasmonic rectangular nanoantennas, that is, rectangular aperture antennas in a gold film, rotated by 45° in the x-y plane. Plasmonic antennas (and their Babinet-inverted configuration), based on the excitation of two resonant modes, can achieve the full phase excursion in the transmission (and reflection) coefficient only on the cross-polarized field. This is possible in view of the property of plasmonic antennas, according to which a rotation by 90° of the antenna in its plane introduces a π phase shift in the cross-polarized scattered light.[22]

Hence, a normally incident, linearly polarized field forming an angle α with the x-axis yields two transmitted beams: an ordinary one, co-polarized, and (ideally) experiencing zero phase gradient; and an anomalous one, with polarization direction rotated by an angle $90° - \alpha$, and experiencing the steering effect imparted by the MS.[10] The two beams are co-polarized for illumination polarized along the symmetry axis ($x = y$) and orthogonally polarized for x- or y-polarized illumination (i.e. $\alpha = 0°$ or 90°, respectively).

The minimum number of antennas per macrocell is two, corresponding to $\Delta\phi = \pi$, which is the maximum sampling step allowing a correct reconstruction of the linear phase profile, though with an uncertainty in the sign of the gradient. This configuration is particularly simple and interesting, since the corresponding macrocell is composed of two antennas with equal dimensions, differing only by a rotation of 90°, which determines a π phase difference in the cross-polarized scattered light. Remarkably, this phase shift is independent on the operation wavelength.[45]

The geometry of the macrocell is shown in Figure 1(b), where the two antennas have the same sidelengths and are rotated by 90°, so that the phase gradient is $\gamma = \pi/d$. As noted in previous study,[7] this configuration admits a simple benchmark which is useful in our study, that is, a gradient-free standard array, consisting of the same antennas but equally oriented; this preserves the properties inherent of the single antenna geometry, but removes the phase-gradient effects. The macrocell of the benchmark array is shown in Figure 1(c).

In our previous research,[7] we showed that a plasmonic Babinet-inverted MS composed by the macrocell in Figure 1(b) (with antenna sidelengths 400 nm and 120 nm, and gold-film thickness $t = 50$ nm) exhibited a sensitivity to local refractive-index variations higher than the corresponding gradient-free benchmark. Here, starting from this result, we carry out a parametric study, in order to assess the effect of the phase gradient and its advantages on gradient-free standard plasmonic arrays. This study will draw the guidelines for the design of high-sensitivity devices based on MSs for label-free biological and chemical sensing applications.

Results and discussion

Our numerical study related to the sensing performance pertaining to phase-gradient and benchmark (gradient-free) configurations is based on the evaluation, from the reflectivity spectral response, of the surface sensitivity S in terms of resonant-wavelength shift due to local refractive changes occurring at the sensor surface. The local refractive changes, here, considered rely on the deposition of a thin (40 nm) SiO_x (refractive index = 1.7) overlay.

Although the selected overlay might not be representative of specific biological molecules, we preferred to maintain the same values we used earlier,[7] in order to facilitate the comparison of the simulated structures with the fabricated ones. However, we verified that the specific values of parameters do not affect qualitatively the results we illustrate hereafter.

All numerical results are obtained by means of a public-domain 2-D implementation (https://sourceforge.net/projects/rcwa-2d/) of the Rigorous Coupled-Wave Analysis.[46] In the simulations, we consider the MS laid over an infinite

(lossless and nondispersive) silica substrate (refractive index = 1.45), while the exterior region is assumed to be air. We use a standard dispersion model for gold[47] and a lossless and nondispersive model for SiOx. The spectra and field profiles are computed by assuming a normally incident plane wave with x-polarized electric field; the convergence is achieved using 51 × 51 modes. In our previous study,[7] this model was found to be in good agreement with experimental results obtained on actual fabricated meta-tip prototypes. The dimensions of the rectangular nanohole antennas (see Figure 1) affect the resonance wavelength (and its visibility), which can be roughly estimated analytically.[48] We maintain fixed such dimensions to 400 nm and 120 nm, in order to focus on the effect of the phase gradient. Specifically, we vary the distance d between the antennas to tune the phase gradient γ, according to equation (3), and the wavelength λ_{SW} of the MS, according to equation (4). Moreover, we vary the gold-film thickness t to shift the resonance wavelengths $\lambda_r^{\mathrm{MS,BC}}$. Here and henceforth, the abbreviations MS and BC refer to the phase-gradient MS or to the benchmark configuration, respectively.

We considered the largest ranges of interest for d and t, and we show the results in terms of sensitivities for d = 530, 700, 1000 nm, and for t = 15, 30, 50, 80 nm. We verified that sampling in a denser way those ranges does not add any useful information.

For all the combinations of chosen values for d and t, we compute numerically the MS and BC sensitivities, defined as

$$S^{\mathrm{MS,BC}} = \frac{\Delta\lambda_r^{\mathrm{MS,BC}}}{\lambda_r^{\mathrm{MS,BC}}} \frac{1}{t_{\mathrm{layer}}} \tag{6}$$

where $\Delta\lambda_r^{\mathrm{MS,BC}}$ is the shift of the resonance wavelength $\lambda_r^{\mathrm{MS,BC}}$ upon the addition of the overlay, and t_{layer} the thickness of the overlay.

Since we are mainly interested to assess the role of phase gradients on the sensing performances of plasmonic arrays, the attention has been focused on the evaluation of the sensitivity gain achieved when using phase-gradient MSs instead of zero-gradient arrays. In Table 1, the values of the sensitivity gain $S^{\mathrm{MS}}/S^{\mathrm{BC}}$ of the MS with respect to the BC are shown for the different configuration analyzed. However, as expected, they increase as the gold thickness decreases,[49] reaching the value of $S^{\mathrm{MS}} = 0.0045\ \mathrm{nm}^{-1}$ for d = 530 nm and t = 15 nm.

As the gold thickness decreases, the resonance wavelengths shift toward higher values,[49] as expected, and, for the MS, they fall at different distances from λ_{SW}. This is shown in Figure 2, where the transmission angle θ_t is plotted as a function of the operation wavelength, according to equation (1). For d = 1000 nm, $\lambda_r^{\mathrm{MS}} < \lambda_{\mathrm{SW}}$, that is, $\theta_t < 90°$ at λ_r^{MS} (see Figure 2), for all thickness values. Note that, for d = 1000 nm, the reflectivity spectra (see panels c and f of Figures 3 and 4) for the MS and the BC configurations are very similar, suggesting that in this case the array effects are negligible, and the reflectivity spectra are affected mainly by the antenna resonance. In this case, the MS exhibits a sensitivity higher by a factor ranging from 1.2 to 1.4 with respect to the BC (see Table 1). For d = 530,700 nm, $\lambda_r^{\mathrm{MS}} \geq \lambda_{\mathrm{SW}}^t$ for all analyzed values of t; this implies that the transmitted cross-polarized field couples to a surface wave for all considered thickness values, and λ_r^{MS} gets further away from λ_{SW} as the gold thickness decreases. Since at λ_{SW} the optimal SPP launching condition is satisfied, this might explain the decrease of the sensitivity gain as t decreases, remaining however always greater than 1. The sensitivity gain has a different behavior for $t \leq 30$ nm and $t \geq 50$ nm as d varies. For $t \leq 30$ nm, as d decreases, the gain decreases as well, which is not coherent with the variation of the distance $|\lambda_r^{\mathrm{MS}} - \lambda_{\mathrm{SW}}|$. On the other hand, for $t \geq 50$ nm, the gain is higher for lower values of d, thereby following the trend of the distance $|\lambda_r^{\mathrm{MS}} - \lambda_{\mathrm{SW}}|$. This behavior might be related to the capability of the metal film to support SPPs,[50] which is poor for low values of the gold thickness and improves for $t \geq 50$ nm (approximately twice the penetration skin depth in the gold layer at the considered wavelengths).

Table 1. Numerically computed sensitivity S^{MS} [10^{-3} nm^{-1}] of the phase-gradient MS (top), and sensitivity gain of the phase-gradient MS with respect to the benchmark $S^{\mathrm{MS}}/S^{\mathrm{BC}}$ (bottom), for different values of the gold-film thickness t and antenna distance d.

t (nm) \ d (nm)	530	700	1000
15	4.5	3.8	4
30	3.8	4	4
50	3.3	3.8	2.8
80	3	3.5	2.5
t (nm) \ d (nm)	530	700	1000
15	1.1	1.1	1.2
30	1.2	1.2	1.3
50	1.4	1.5	1.4
80	1.7	1.8	1.4

The gain in sensitivity is likely attributable to a field enhancement on the surface of the structure,[7] as it can be observed in Figure 5, where the field intensity profile over a single antenna is shown for d = 530 nm and t = 15 and 80 nm. A larger ratio between the maxima of the field profiles of the MS and the BC configurations corresponds to a higher sensitivity gain. Indeed, the higher the field, the stronger its interaction with the external environment, and hence the higher the wavelength shift (see e.g. Harrington's textbook[51]).

In Figures 3 and 4, the spectra computed for the MS and the BC for t = 15, 50 nm and d = 530, 700, and 1000 nm are shown. The other spectra are omitted for brevity.

From the inspection of these spectra, it is clear that the MS outperforms the BC also in terms of fringe visibility

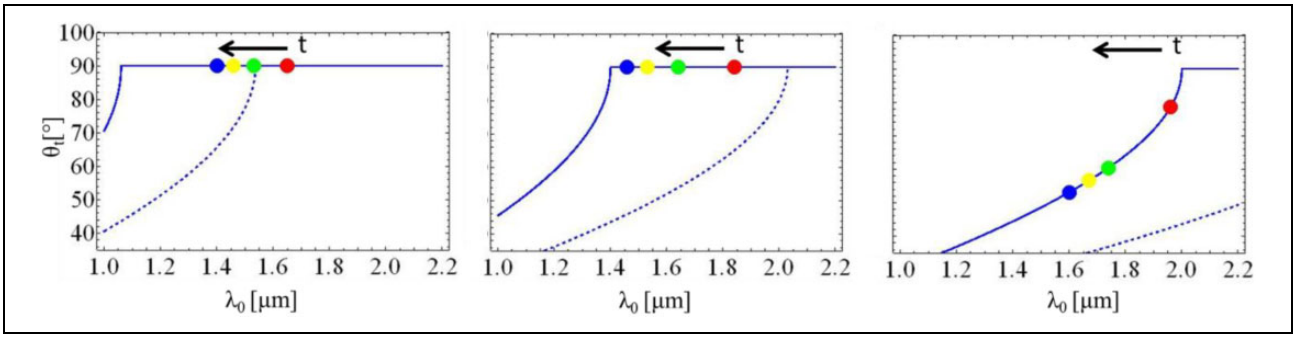

Figure 2. Refraction (solid line) and reflection angle (dashed line) versus wavelength according to equation (1) for $d = 530$ nm (left); $d = 700$ nm (center); $d = 1000$ nm (right).The bullets indicate the resonance wavelength of the MS for the different thickness values t considered in Table 1; the black arrow indicates the direction of increasing t. MS: metasurface.

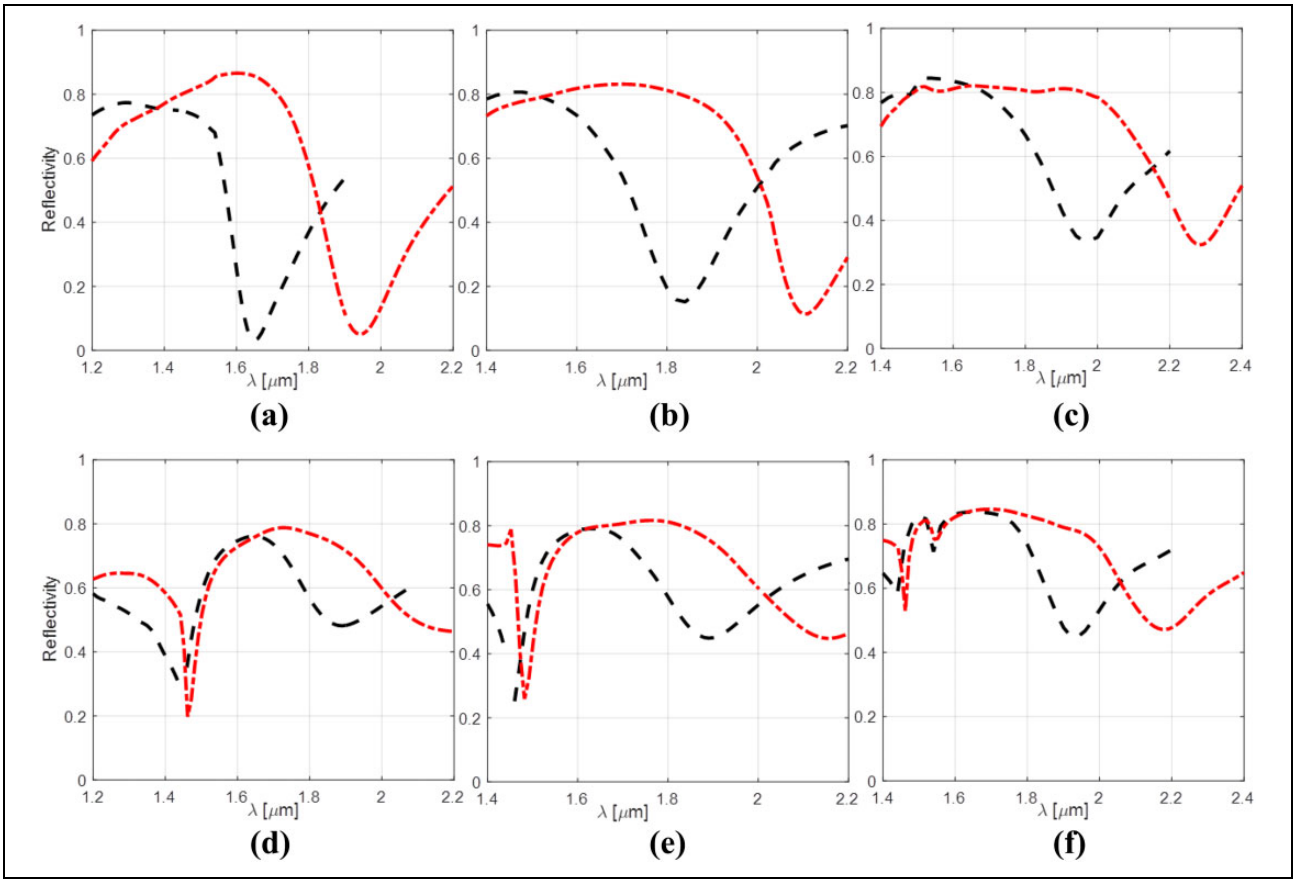

Figure 3. Numerically evaluated reflectivity spectra of the MS ((a) to (c)) and the BC ((d) to (f)), assuming a normally incident plane wave with x-polarized electric field, for gold-film thickness $t = 15$ nm, and three values of the distance between antennas $d = 530$ nm (a and d); $d = 700$ nm (b and e); $d = 1000$ nm (c and f). Red-dash-dotted and black-dashed curves pertain to structures with and without the deposition of a 40-nm overlay of SiO_x (refractive index: 1.7). MS: metasurface.

and width of the resonance band, especially for $d = 530$ nm and $t = 15$, 30 nm, for which also the reflected anomalous beam couples to a surface wave (see Figure 2). This effect might be due to the interplay between the surface waves excited at the two sides of the metal film.

To sum up, the results from this study confirm that the phase gradient can be effectively exploited as an additional degree of freedom in the design of high-performance sensors based on plasmonic arrays. Indeed, we show that the simple introduction of a constant phase gradient always yields a gain with respect to the corresponding zero-gradient benchmark. The gain in sensitivity increases as the resonance wavelength approaches λ_{SW}, that is, the grazing-refraction condition ($\theta_t = 90^\circ$); the performance of the MS-based sensor could also be improved if the

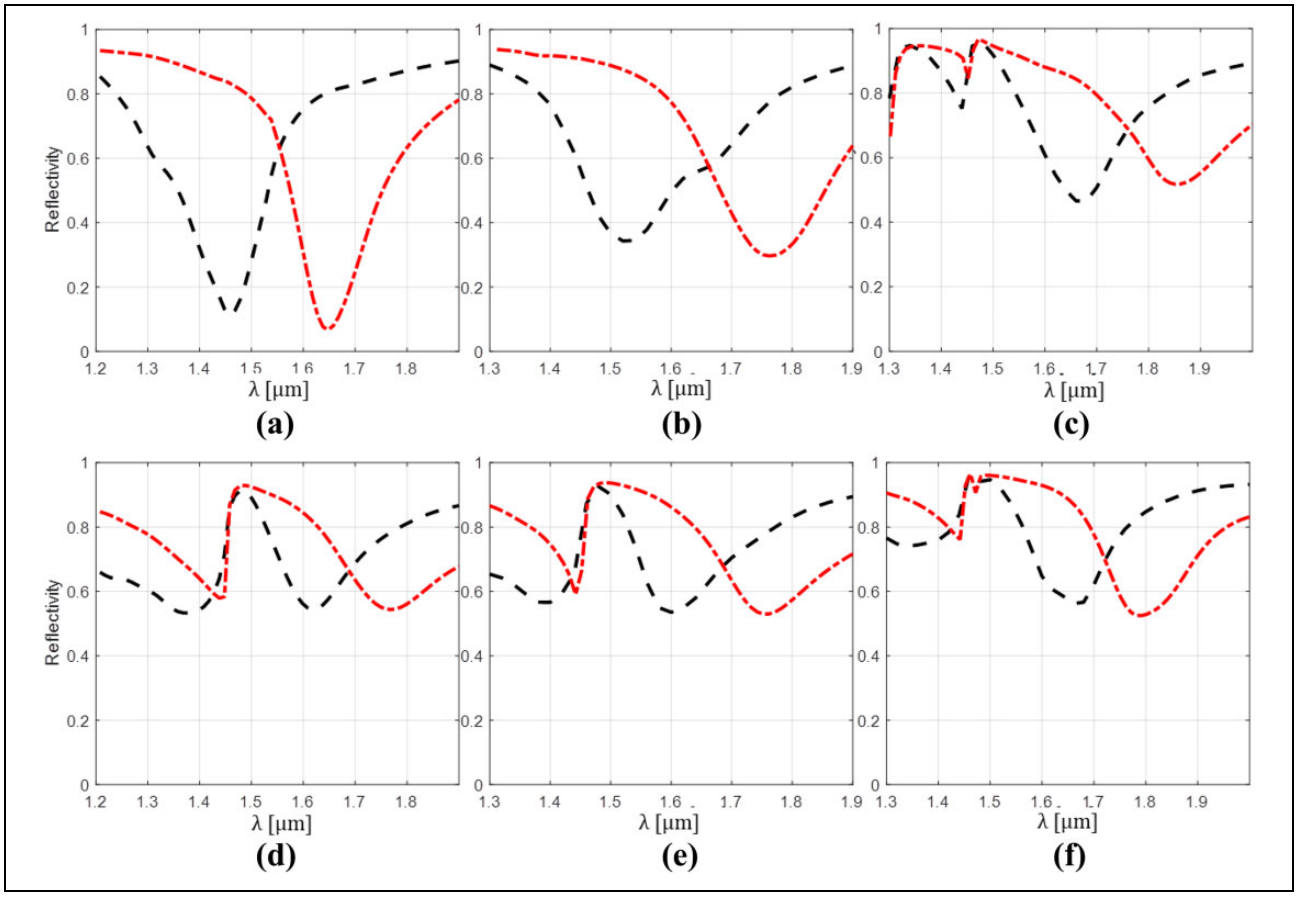

Figure 4. As in Figure 3, but for gold-film thickness $t = 50$ nm.

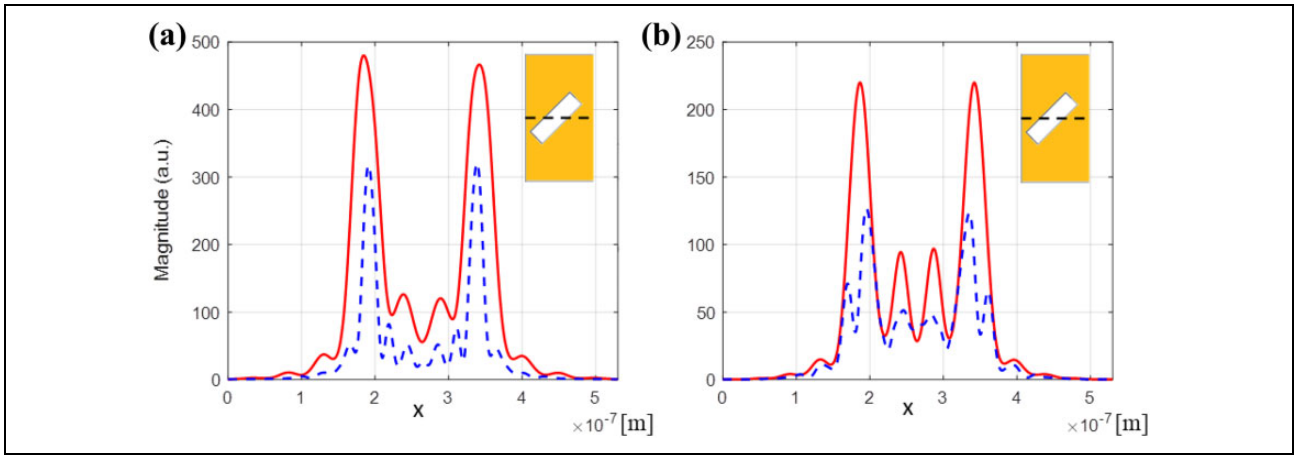

Figure 5. Numerically evaluated electric field intensity profile over the dashed line on the antenna (inset) at the gold–air interface for gold thickness $t = 15$ nm (a), and $t = 80$ nm (b) for the MS (red solid) and the BC (blue dashed). MS: metasurface.

resonance wavelength approaches the grazing-reflection condition ($\theta_r = 90°$) too.

Conclusions

Building upon our previous results,[7] we have conducted a parametric study to evaluate the effect of a linear phase profile in plasmonic MS on the surface sensitivity, to pave the way for using fiber-optic meta-tips for label-free biological and chemical sensing. For fixed antenna dimensions, we have varied the (constant) phase gradient to couple the impinging field to a surface wave, by varying the distance between antennas, and the distance between the resonance wavelength of the structure and the surface-wave-coupling

wavelength. To assess the role of the phase gradient, we have compared the sensing performance with those pertaining to a gradient-free benchmark structure. Our results indicate that the phase-gradient MS always exhibits a sensitivity gain, which increases as the resonance wavelength approaches the grazing-refraction condition. When the resonance wavelength also approaches the grazing-reflection condition, there is a sensible improvement in the spectral width and visibility of the resonance.

These outcomes indicate that the phase gradient represents an additional useful degree of freedom in the design of a meta-tip sensing platform, by generally improving the figures of merit and adding only very mild complexity to the fabrication process.

This study provides several hints, summarized above, and specifically that the phase-gradient MS always exhibits a sensitivity gain for different values of the gold-film thickness and antenna distance. Based on these results, it will be possible to design high-sensitivity MS-based devices for specific biochemical sensing applications, including a specific external environment and a specific range where the resonance wavelengths must lie.

In particular, as standard (gradient-free) plasmonic fiber tip–based biosensors have been demonstrated to be able to reach ultimate performance (e.g. femtomolar and picomolar limits of detection) in different cancer biomarker detection applications,[52,53] our results pave the way to the design and development of extremely high-sensitivity optical fiber meta-tips that could potentially outperform already reported gradient-free fiber-based devices.

Declaration of conflicting interests

The author(s) declared no potential conflicts of interest with respect to the research, authorship, and/or publication of this article.

Funding

This work was supported in part by PRIN project "Lab on fIber technology For advanced optical nanoprobEs - LIFE" and by Progetto POR Campania "Nanofotonica Per La Lotta Al Cancro - NANOCAN".

References

1. Brolo AG. Plasmonics for future biosensors. *Nature Photon* 2012; 6: 709–713.
2. Li M, Cushing SK, and Wu N. Plasmon-enhanced optical sensors: a review. *Analyst* 2015; 140: 386–406.
3. Guo L, Jackman JA, Yang HH, et al. Strategies for enhancing the sensitivity of plasmonic nanosensors. *Nano Today* 2015; 10: 213–239.
4. Albert JA. Lab on fiber. *IEEE Spectrum* 2014; 51: 48–53.
5. Kostovski G, Stoddart PR, and Mitchell A. The optical fiber tip: an inherently light-coupled microscopic platform for micro-and nanotechnologies. *Adv Mater* 2014; 26: 3798–3820.
6. Cusano A, Consales M, Crescitelli A, et al. *Lab-on-fiber technology*. Vol. 56. Berlin: Springer, 2015.
7. Principe M, Consales M, Micco A, et al. Optical fiber meta-tips. *Light Sci Appl* 2017; 6: e16226–e16236.
8. Capolino F. *Theory and phenomena of metamaterials*. Boca Raton: CRC Press, 2009.
9. Kildishev AV, Boltasseva A, and Shalaev VM. Planar photonics with metasurfaces. *Science* 2013; 339: 139–150.
10. Yu N, Genevet P, Aieta F, et al. Flat optics: controlling wavefronts with optical antenna metasurfaces. *IEEE J Select Topics Quantum Electron* 2013; 19: 4700423–4700423.
11. Yu N and Capasso F. Flat optics with designer metasurfaces. *Nature Mater* 2014; 13: 139–150.
12. Aieta F, Genevet P, Kats MA, et al. Aberration-free ultrathin flat lenses and axicons at telecom wavelengths based on plasmonic metasurfaces. *Nano Lett* 2012; 12: 4932–4936.
13. Aieta F, Kats MA, Genevet P, et al. Multiwavelength achromatic metasurfaces by dispersive phase compensation. *Science* 2015; 347: 1342–1345.
14. Yang Y, Kravchenko II, Briggs DP, et al. All-dielectric metasurface analogue of electromagnetically induced transparency. *Nat Commun* 2014; 5: 5753–5759.
15. Zhang X and Wu Y. Effective medium theory for anisotropic metamaterials. *Sci Rep* 2015; 5: 7892–7899.
16. Silva A, Monticone F, Castaldi G, et al. Performing mathematical operations with metamaterials. *Science* 2014; 343: 160–163.
17. Pors A, Nielsen MG, and Bozhevolnyi SI. Analog computing using reflective plasmonic metasurfaces. *Nano Lett* 2015; 15: 791–797.
18. Berry DC, Malech RG, and Kennedy W. The reflectarray antenna. *IEEE Trans Antennas Propagat* 1963; 11: 645–651.
19. McGrath D. Planar three-dimensional constrained lenses. *IEEE Trans Antennas Propagat* 1986; 34: 46–50.
20. Meinzer N, Barnes WL, and Hooper IR. Plasmonic meta-atoms and metasurfaces. *Nature Photon* 2014; 8: 889–898.
21. Zou L, Withayachumnankul W, Shah CM, et al. Dielectric resonator nanoantennas at visible frequencies. *Opt Expr* 2013; 21: 1344–1352.
22. Yu N, Genevet P, Kats MA, et al. Light propagation with phase discontinuities: generalized laws of reflection and refraction. *Science* 2011; 334: 333–337.
23. Memarzadeh B and Mosallaei H. Array of planar plasmonic scatterers functioning as light concentrator. *Opt Lett* 2011; 36: 2569–2571.
24. Ni X, Emani NK, Kildishev AV, et al. Broadband light bending with plasmonic nanoantennas. *Science* 2010; 335: 427–427.
25. Pfeiffer C and Grbic A. Metamaterial Huygens' surfaces: tailoring wave fronts with reflectionless sheets. *Phys Rev Lett* 2013; 110: 197401–197405.
26. Monticone F, Estakhri NM, and Alù A. Full control of nanoscale optical transmission with a composite metascreen. *Phys Rev Lett* 2013; 110: 203903–203908.

27. Ni X, Ishii S, Kildishev AV, et al. Ultra-thin, planar, Babinet-inverted plasmonic metalenses. *Light Sci Appl* 2013; 2: e72–e78.
28. Farmahini-Farahani M and Mosallaei H. Birefringent reflectarray metasurface for beam engineering in infrared. *Opt Lett* 2013; 38: 462–464.
29. Alrasheed S and Di Fabrizio E. Plasmonic nanospherical dimers for color pixels. *Nanomater Nanotechno* 2018; 8: 1–7.
30. Lin D, Fan P, Hasman E, et al. Dielectric gradient metasurface optical elements. *Science* 2014; 345: 298–302.
31. Kim M, Wong AMH, and Eleftheriades GV. Optical Huygens' metasurfaces with independent control of the magnitude and phase of the local reflection coefficients. *Phys Rev X* 2014; 4: 041042–041052.
32. Cheng J, Ansari-Oghol-Beig D, and Mosallaei H. Wave manipulation with designer dielectric metasurfaces. *Opt Lett* 2014; 39: 6285–6288.
33. Ding X, Monticone F, Zhang K, et al. Ultrathin pancharatnam-berry metasurface with maximal cross-polarization efficiency. *Adv Mater* 2015; 27: 1195–1200.
34. Decker M, Staude I, Falkner M, et al. High-efficiency dielectric Huygens' surfaces. *Adv Opt Mater* 2015; 3: 813–820.
35. Arbabi A, Horie Y, Bagheri M, et al. Dielectric metasurfaces for complete control of phase and polarization with subwavelength spatial resolution and high transmission. *Nat Nanotechnol* 2015; 10: 937–943.
36. Lee Y, Kim SJ, Park H, et al. Metamaterials and metasurfaces for sensor applications. *Sensors* 2017; 17: 1726–1753.
37. Sun S, He Q, Xiao S, et al. Gradient-index meta-surfaces as a bridge linking propagating waves and surface waves. *Nat Mater* 2012; 11: 426–431.
38. Sun W, He Q, Sun S, et al. High-efficiency surface plasmon meta-couples: concept and microwave-regime realizations. *Light Sci Appl* 2016; 5: e16003–e16008.
39. Estakhri NM and Alù A. Wave-front transformation with gradient metasurfaces. *Phys Rev X* 2016; 6: 041008–041024.
40. Asadchy VS, Albooyeh M, Tcvetkova SN, et al. Perfect control of reflection and refraction using spatially dispersive metasurfaces. *Phys Rev B* 2016; 94: 075142–07554.
41. Tcvetkova SN, Kwon DH, Diaz-Rubio A, et al. Near-perfect conversion of a propagating plane wave into a surface wave using metasurfaces. *Phys Rev B* 2018; 97: 115447–115457.
42. Serdyukov AN, Semchencko IV, Tretyakov SA, et al. *Electromagnetics of bi-anisotropic materials: theory and applications*. Amsterdam: Gordon and Breach Science, 2001.
43. Larouche S and Smith DR. Reconciliation of generalized refraction with diffraction theory. *Opt Lett* 2012; 37: 2391–2393.
44. Zou C, Withayachumnankul W, Shadrivov IV, et al. Directional excitation of surface plasmons by dielectric resonators. *Phys Rev B* 2015; 91: 085433–085440.
45. Berry MV. The adiabatic phase and Pancharatnam's phase for polarized light. *J Mod Opt* 1987; 34: 1401.
46. Moharam MG, Grann EB, Pommet DA, et al. Formulation for stable and efficient implementation of the rigorous coupled-wave analysis of binary gratings. *J Opt Soc Am A* 1995; 12: 1068–1076.
47. Johnson PB and Christy RW. Optical constants of the noble metals. *Phys Rev B* 1972; 6: 4370–4379.
48. Puscasu I, Spenser D, and Boreman GD. Refractive-index and element-spacing effects on the spectral behavior of infrared frequency-selective surfaces. *Appl Opt* 2000; 39: 1570–1574.
49. Ricciardi A, Consales M, Quero G, et al. Lab-on-fiber devices as an all around platform for sensing. *Opt Fiber Technol* 2013; 19: 772–784.
50. Crescitelli A, Ricciardi A, Consales M, et al. Nanostructured metallo-dielectric quasi-crystals: towards photonic-plasmonic resonance engineering. *Adv Funct Mater* 2012; 22: 4389–4398.
51. Harrington RF. *Time-Harmonic electromagnetic fields,* September 2001. New York: Wiley-IEEE Press. ISBN: 978-0-471-20806-8.
52. Sanders M, Lin Y, Wei J, et al. An enhanced LSPR fiber-optic nanoprobe for ultrasensitive detection of protein biomarkers. *Biosensors and Bioelectronics* 2014; 61: 95–101.
53. Vaiano P, Carotenuto B, Pisco M, et al. Lab on fiber technology for biological sensing applications. *Laser Photonics Rev* 2016; 10: 922–961.